 doi:10.20944/preprints202203.0357.v1

Type of the Paper (Article)

Negative Electrical Conductivity Metamaterials

Edward Bormashenko

Ariel University, Ariel, 407000, Israel, Engineering Faculty, Department of Chemical Engineering, Biotechnology and Materials, edward@ariel.ac.il

Abstract: The system of non-interacting electrically charged core-massless spring-shell mechanical units, demonstrating negative effective mass, is considered, seen as a Drude-Lorentz gas. When such an ideal gas is exposed to the external harmonic field, it demonstrates as the certain conditions the negative frequency-dependent electrical conductivity. The negative value of the electrical conductivity σ implies that the electrical current will flow against the direction of the electric field and correspondingly the direction of the electrical force. Low- and high-frequency asymptotic behavior of the electrical conductivity is addressed. The same system demonstrates at low frequencies the negative asymptotic refraction. Experimental realization of the introduced model system, based on the exploitation of plasma oscillations of the free electron gas is suggested.

Keywords: metamaterial; negative electrical conductivity; negative mass; Drude-Lorentz model; negative refraction.

1. Introduction

Development of metamaterials opened novel and broad horizons for the materials science [1-9]. Metamaterials are usually defined as engineered, artificial, periodic composites for altering electromagnetic [2, 5-6], mechanic [7] or thermal [9] properties of materials to obtain properties that are not observed naturally. The prefix *meta* (a Greek word meaning 'beyond') indicates that the characteristics of the material are beyond what we see in nature. The macroscopic structural units of the metamaterials of the metamaterial – can be tailored in shape and size, the lattice constant and inter-unit interaction can be artificially tuned, and "defects" can be precisely designed and placed at desired locations. Numerous contra-intuitive effects such as an effect of the negative refraction [10 and negative effective mass became possible with the meta-materials [11-16]. The effect of the negative effective mass may be attained under exploiting the plasma oscillations of the electron gas in metals [15-16]. The negative effective mass materials were already successfully demonstrated experimentally by embedding soft silicon rubber coated heavy spheres in epoxy, acting as the local mechanical resonators [17]. Metamaterials offer the potential to precise control of the pathway of propagation of a wave (electromagnetic or acoustic) in a material. Metamaterials can also be customized to support novel properties that currently are not accessible with existing optical and acoustic hardware [18]. Development of metamaterials enabled numerous engineering applications, including optical camouflage and invisibility cloaks, optical, acoustic and thermal cloaking [19-21]. Our paper is devoted to the possibility of realization of negative thermal conductivity meta-materials, which were introduced recently in ref. 22. We suggest the model meta-material system demonstrating negative electrical conductivity emerging from the negative effective mass of the charge carriers.

2. Results

2.1. Negative electrical conductivity in the system of the charged core-shell units

Preprints (www.preprints.org) | NOT PEER-REVIEWED | Posted: 28 March 2022 doi:10.20944/preprints202203.0357.v1

Consider the ideal gas of the core-ideal spring -shell units embedded into the matrix of obstacles depicted in **Figure 1**. Core-spring-shell units shown in **Figure 1** give rise to the effect of negative effective mass effect, as demonstrated in refs. 11-14. A core with mass m is connected via the Hookean massless spring with constant k to a spherical shell with mass M. When the system is subjected to the external sinusoidal force $\boldsymbol{F(t) = F_0 sin\omega t}$ it may be replaced with a single effective mass $\boldsymbol{m_{eff}}$ expressed with Eq. 1 (for the rigorous derivation of Eq. 1. see refs.11-16):

$$m_{eff} = M + \frac{m\omega_0^2}{\omega_0^2 - \omega^2} \tag{1}$$

$\vec{E}(t) = \vec{E}_{ox} e^{-j\omega t}$

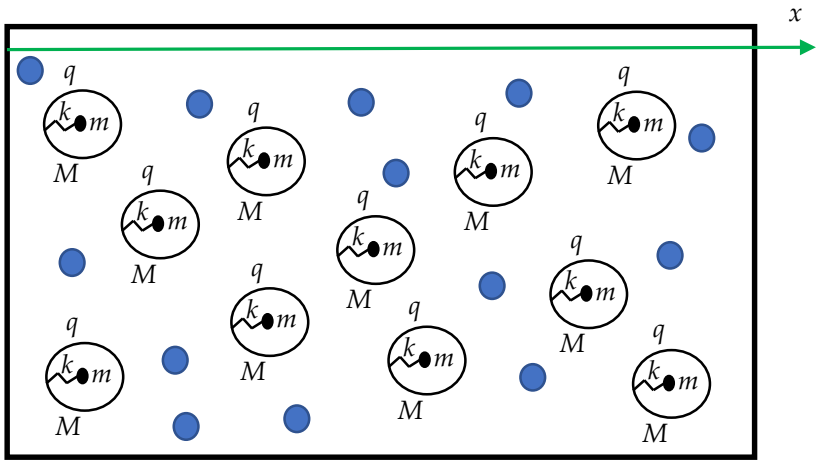

Figure 1. Ideal gas of "negative mass units" carrying the electrical charge q exposed to the external electric field $\vec{E}(t) = \vec{E}_{ox} e^{j\omega t}$. Negative mass units are built from the core with mass m is connected through the spring with constant k to a spherical shell with mass M. Blue circles depict the "obstacles".

where $\boldsymbol{\omega_0 = \sqrt{\frac{k}{m}}}$. It is easily recognized from Eq. 1 that, when the frequency $\boldsymbol{\omega}$ approaches $\boldsymbol{\omega_0}$ from above the effective mass $\boldsymbol{m_{eff}}$ will be negative [11-16]. The core-shell units are supposed to be non-interacting; thus, the "gas" shown in **Figure 1** is treated as an ideal one. Now we assume that the shell M is electrically charged with the electrical charge q (it should be emphasized, that the core m is supposed to be neutral, thus the total excess electrical charge of the system is q). The entire system is embedded into the lattice of fixed "obstacles", depicted in **Figure 1** with a blue circles. We treat the system within the simplest possible framework of the Drude-Lorentz theory, assuming that the behavior of the charged core-apring-shell systems (resembling electrons in the Drude-Lorentz model) dispersed between the obstacles (resembling in turn immobile ions in the classical electron theory) may be treated classically and behaves much like a pinball machine, with a gas of constantly jittering charged core-shell units bouncing and re-bouncing off heavier, relatively immobile obstacles [23-24].

Now we expose the suggested model system to the external field $\boldsymbol{\vec{E}(t) = \vec{E}_{ox} e^{-j\omega t}}$,

which will give rise to the electrical current density $\boldsymbol{\vec{J}}$. The Drude-Lorentz classical theory predicts for the relationship between $\boldsymbol{\vec{J}}$ and $\boldsymbol{\vec{E}}$ Eq. 2:

$$\boldsymbol{\vec{J} = \frac{nq^2\tau}{m_{eff}} \vec{E}} \ , \tag{2}$$

Preprints (www.preprints.org) | NOT PEER-REVIEWED | Posted: 28 March 2022 doi:10.20944/preprints202203.0357.v1

where n and τ are respectively the number density of core-shell units and mean free time between collisions of the core-shell units with the "obstacles" respectively. Eq. 2 deserves a more deep analysis. It should be emphasized, that the addressed model system has two characteristic time scales, namely $\boldsymbol{\tau}$ and $\frac{1}{\omega_0}$. The core-spring-shell unit charge carrier is exposed to the complex force $\hat{\boldsymbol{F}}(\boldsymbol{t}) = \boldsymbol{qE_{ox}e^{-j\omega t}}$ driving the charge carriers and this giving rise to the complex current density $\hat{\boldsymbol{J}}$ supplied by Eq. 2. The very question is: why the effective mass denoted $\boldsymbol{m_{eff}}$ should appear in Eq. 2 instead of the mass of the charge carrier? Derivation of Eq. 2 within the Drude-Lorentz model assumptions implies that Eq. 3, predicting the complex moment of the charge carrier is true:

$$\hat{\boldsymbol{P}} = \boldsymbol{m_{eff}}\hat{\boldsymbol{V}} \tag{3}$$

where $\hat{\boldsymbol{P}}$ is the entire complex moment of the core-spring-shell system, $\hat{\boldsymbol{V}}$ is the complex velocity of the shell and $\boldsymbol{m_{eff}}$ is given by Eq. 1 (the notation of vector is omitted for brevity in Eq. 3; for details of rigorous derivation of Eq. 3 see ref. 11). Actually, Eq. 3 expresses the second Newton law for the entire core-shell system, which is exploited in the classical Drude-Lorentz model for the derivation of Eq. 2. It should be emphasized that the charge transport arises from the motion of the entire core-spring-shell system, represented by the effective mass $\boldsymbol{m_{eff}}$; in other words we substitute the complex mechanic system by the effective mass $\boldsymbol{m_{eff}}$ charged with electrical charge q. This consideration and taking into acTcount Eq. 2 justifies appearance of the effective mass $\boldsymbol{m_{eff}}$ in Eq. 2. Eq. 1 and Eq. 2 immediately predict for the electrical conductivity $\boldsymbol{\sigma}$ of the model system shown in **Figure 1** the following expression:

$$\boldsymbol{\sigma(\omega)} = \frac{\boldsymbol{nq^2\tau}}{\boldsymbol{m_{eff}}} = \frac{\boldsymbol{nq^2\tau}}{\boldsymbol{M}+\frac{\boldsymbol{m\omega_0^2}}{\boldsymbol{\omega_0^2-\omega^2}}} \tag{4}$$

It is easily recognized from Eq. 1 and Eq. 4. that, when the frequency $\boldsymbol{\omega}$ approaches $\boldsymbol{\omega_0}$ from above the electrical conductivity $\boldsymbol{\sigma}$ will be negative. What does it mean physically? The negative value of the electrical conductivity $\boldsymbol{\sigma}$ implies that the electrical current will flow against the direction of the electric field $\vec{\boldsymbol{E}}$ and correspondingly the electrical force $\vec{\boldsymbol{F}} = \boldsymbol{q}\vec{\boldsymbol{E}}$.

It us useful to supply the low-frequency, high-frequency limits of electrical conductivity, and the asymptotic value of $\boldsymbol{\sigma}$ in the vicinity of $\boldsymbol{\omega_0} = \sqrt{\frac{\boldsymbol{k}}{\boldsymbol{m}}}$:

$$\lim_{\boldsymbol{\omega\to 0}} \boldsymbol{\sigma(\omega)} = \frac{\boldsymbol{nq^2\tau}}{\boldsymbol{M+m}} = \frac{\boldsymbol{nq^2\tau}}{\boldsymbol{M_{tot}}}, \tag{5}$$

$$\lim_{\boldsymbol{\omega\to\omega_0}} \boldsymbol{\sigma(\omega)} = \boldsymbol{\left(\omega_0^2 - \omega^2\right)}\frac{\boldsymbol{nq^2\tau}}{\boldsymbol{m\omega_0^2}}, \tag{6}$$

$$\lim_{\boldsymbol{\omega\to\infty}} \boldsymbol{\sigma(\omega)} = \frac{\boldsymbol{nq^2\tau}}{\boldsymbol{M}}, \tag{7}$$

where $\boldsymbol{M_{tot}} = \boldsymbol{M} + \boldsymbol{m}$ is the total mass of the core-shell unit (the mass of the spring is zero). It is noteworthy, that the low-frequency, high-frequency limits of the electrical conductivity are independent of the frequency of the external electric field $\boldsymbol{\omega}$. It is also should be noted, that the high=frequency limit of the electrical conductivity is independent of the core-mass m.

2.2. Refractive index of the suggested model gas built of charged core-shell units

Preprints (www.preprints.org) | NOT PEER-REVIEWED | Posted: 28 March 2022 doi:10.20944/preprints202203.0357.v1

The squared refractive index n of the suggested model ideal gas built of charged core-shell units, shown in **Figure 1**, is given within the classical Drude-Lorentz model by Eq. 8:

$$\boldsymbol{n^2(\omega) = 1 + \frac{\sigma}{\varepsilon_0 j\omega(1+j\omega\tau)} = 1 + \frac{nq^2\tau}{\varepsilon_0 j\left(M+\frac{m\omega_0^2}{\omega_0^2-\omega^2}\right)\omega(1+j\omega\tau)}} \quad , \tag{8}$$

arising from the basic assumptions of the Drude-Lorentz model [23-25] and Eq. 4. Eq. 8 is a somewhat cumbersome one. Consider, first, the asymptotic behavior of the refractive index $\boldsymbol{n(\omega)}$ in the high-frequency limit, i.e. in the limit of $\boldsymbol{\omega\tau \gg 1}$, given by Eq. 9:

$$\boldsymbol{n^2(\omega) = 1 - \frac{nq^2}{\varepsilon_0\left(M+\frac{m\omega_0^2}{\omega_0^2-\omega^2}\right)\omega^2}} \tag{9}$$

Remarkably, the high-frequency limit of the refractive index, supplied by Eq. 9, is independent of the characteristic time scale τ. Now, consider asymptotic behavior of the refractive index in the vicinity of the frequency $\boldsymbol{\omega_0}$ (this implies: $\boldsymbol{\omega\tau \gg 1; \omega_0\tau \gg 1}$), expressed by Eq. 10:

$$\boldsymbol{\lim_{\omega\tau\gg 1;\omega\to\omega_0} n^2(\omega) = 1 - \frac{nq^2}{\varepsilon_0 m}\frac{\omega_0^2-\omega^2}{\omega^2}} \tag{10}$$

Eq. 10 is valid when the interrelation between the characteristic time scales given by $\boldsymbol{\tau \gg \frac{1}{\omega_0}}$ takes place (we emphasize the twin time-scale nature of the introduced model). It is also recognized from Eq. 10, that the asymptotic value of the refractive index in the vicinity of the high frequency $\boldsymbol{\omega_0}$ is independent not only of the characteristic time scale τ but also of the shell mass M, being dependent on the core mass m, the spring constant k ($\boldsymbol{\omega_0 = \sqrt{\frac{k}{m}}}$) and the number density of the core-shell units n. It is seen from Eq. 10 that for $\boldsymbol{\omega < \omega_0}$ we have for the aforementioned asymptotic $\boldsymbol{n < 1}$, whereas when the frequency $\boldsymbol{\omega}$ approaches $\boldsymbol{\omega_0}$ from above $\boldsymbol{n > 1}$ takes place. It is also recognized from Eq. 10 that the high-frequency asymptotic of the refractive index is real (the imaginary component of n is absent), which is typical for metals which are transparent for high frequencies (low wavelengths).

It is also instructive to calculate the low-frequency limit of the refraction index (now $\boldsymbol{\omega\tau \ll 1}$ is adopted). In this case, combining of Eq. 8 and Eq. 4 yields:

$$\boldsymbol{n^2(\omega) \cong 1 - j\frac{\sigma}{\varepsilon_0\omega} \cong -j\frac{\sigma}{\varepsilon_0\omega} = -\frac{j}{\varepsilon_0\omega}\frac{nq^2\tau}{M+\frac{m\omega_0^2}{\omega_0^2-\omega^2}}} \tag{11}$$

Consider now the asymptotic behavior of the low-frequency limit of the refractive index, when $\boldsymbol{\omega \to \omega_0}$ is assumed.

$$\boldsymbol{\lim_{\omega\tau\ll 1;\omega\to\omega_0} n^2(\omega) = -j\frac{nq^2\tau}{\varepsilon_0\omega}\frac{\omega_0^2-\omega^2}{m\omega_0^2}} \tag{12}$$

Now, the interrelation between the characteristic time scales given by $\boldsymbol{\tau \ll \frac{1}{\omega_0}}$ takes place. Considering $\boldsymbol{\sqrt{-j} = \frac{1-j}{\sqrt{2}}}$ yields Eq. 13:

$$\boldsymbol{\lim_{\omega\tau\ll 1;\omega\to\omega_0} n(\omega) = -(j+1)\sqrt{\frac{nq^2\tau}{2\varepsilon_0 m\omega\omega_0^2}}\sqrt{\omega^2-\omega_0^2} = n_R(\omega) + jn_I(\omega)}, \tag{13}$$

Preprints (www.preprints.org) | NOT PEER-REVIEWED | Posted: 28 March 2022 doi:10.20944/preprints202203.0357.v1

where $\boldsymbol{n_R(\omega)}$ are $\boldsymbol{n_I(\omega)}$ are the real and imaginary components of the refractive index correspondingly. Let take a close look on Eq. 13: first of all we conclude that $|\boldsymbol{n_R(\omega)}| = |\boldsymbol{n_I(\omega)}|$ takes place and this is typical for the low-frequency asymptotic of the refractive index in metals [25]. The asymptotic value of the real component of the refractive index, when $\boldsymbol{\omega \to \omega_0}$ is assumed, is given in turn by Eq. 14:

$$\lim_{\omega\tau\ll 1;\omega\to\omega_0} \boldsymbol{n_R(\omega)} = -\sqrt{\frac{nq^2\tau}{2\varepsilon_0 m\omega\omega_0^2}}\sqrt{\omega^2-\omega_0^2} \cong -\sqrt{\frac{nq^2\tau}{2\varepsilon_0 m\omega_0}}\sqrt{\left(\frac{\omega}{\omega_0}\right)^2-1} \quad (14)$$

Again, Eq. 14 is valid when $\boldsymbol{\tau \ll \frac{1}{\omega_0}}$ is adopted. Remarkably $\boldsymbol{n_R(\omega) < 0}$ takes place when the frequency $\boldsymbol{\omega}$ approaches $\boldsymbol{\omega_0}$ from above; thus, we conclude that the phenomenon of the negative mass may give rise to the negative refraction. And, again, the low frequency asymptotic of the refractive index does not depend on the shell mass *M*, being dependent on the core mass *m* and the number density of the charge carriers only (see Eq. 13).

2.3. Experimental implementation of the suggested model system demonstrating negative thermal conductivity and negative refraction

The very question is: how the suggested model system, depicted in **Figure 1**, demonstrating negative thermal conductivity and negative refraction may be realized experimentally? We already suggested the negative effective mass metamaterial based on the electro-mechanical coupling exploiting plasma oscillations of a dilute free electron gas, immersed into a lattice of fixed positively charged ions [15, 16]. The negative mass appeared as a result of excitation of a metallic particle with an external frequency ω which is close to the frequency of the plasma oscillations of the electron gas $\boldsymbol{m}$ (denoted $\boldsymbol{\omega_p}$) relatively to the immobile ionic lattice *M*. The plasma oscillations are represented with the elastic spring constant $\boldsymbol{k = \omega_p^2 m}$, where $\boldsymbol{\omega_p}$ is the plasma frequency, as illustrated with **Figure 2**. Thus, the metallic particle excited with the external frequency ω is described by the effective mass $\boldsymbol{m_{eff} = M + \frac{m\omega_p^2}{\omega_p^2-\omega^2}}$, which is negative when the excitation frequency denoted $\boldsymbol{\omega}$ approaches $\boldsymbol{\omega_p}$ from above [15-16]. The model was exemplified with two conducting metals, namely Au and Li particles immersed into various matrices [15-16].

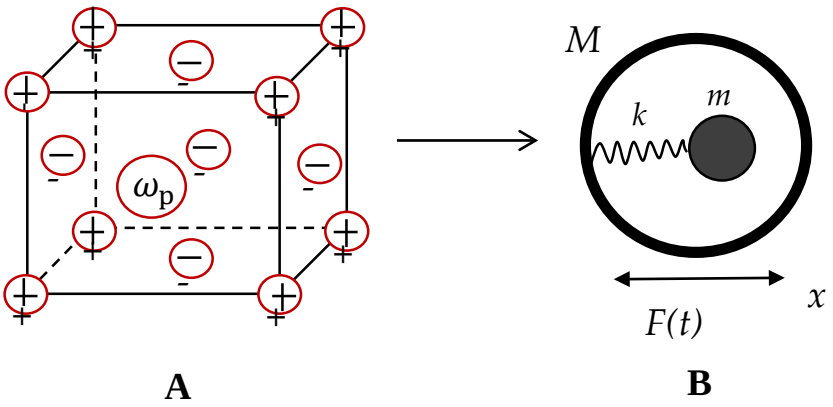

Figure 2. The core-shell system utilizing oscillations of electron gas *m* embedded into the ionic matrix *M*; the oscillations take place with the plasma frequencyω_p, as shown in inset **A**. The equivalent mechanical scheme of the oscillations of the electron gas is illustrated with inset **B**.

Preprints (www.preprints.org) | NOT PEER-REVIEWED | Posted: 28 March 2022 doi:10.20944/preprints202203.0357.v1

Plasma oscillations are represented by the effective spring $k = m\omega_p^2$. When the entire system is exerted to the harmonic external force $F(t) \sim e^{-j\omega t}$ the effective mass is given by: $m_{eff} = M + \frac{m\omega_0^2}{\omega_p^2 - \omega^2}$ [11-16].

Now consider the dilute gas of charged metallic (or semiconductor) micro- or nano-particles immersed into the system of the fixed obstacles, depicted in **Figure 3** with the blue circles. The entire system is exerted to the external electrical field $\vec{\boldsymbol{E}} = \vec{\boldsymbol{E}}_{ox}\boldsymbol{e}^{-j\omega t}$. The particles are charged with the excess electrical charge q. The suggested system resembles the dusty plasma seen as a two- component system composed of negatively charged dust grains and ions [27-29]. Excess electrical charge also may be supplied to the micro-grains by the cold plasma treatment [30]. Similarly to Eq. 4 we obtain for the electrical conductivity of the model material, shown in **Figure 3**:

$$\boldsymbol{\sigma} = \frac{\boldsymbol{nq^2\tau}}{\boldsymbol{m_{eff}}} = \frac{\boldsymbol{nq^2\tau}}{\boldsymbol{M + \frac{m\omega_p^2}{\omega_p^2 - \omega^2}}} \quad (15)$$

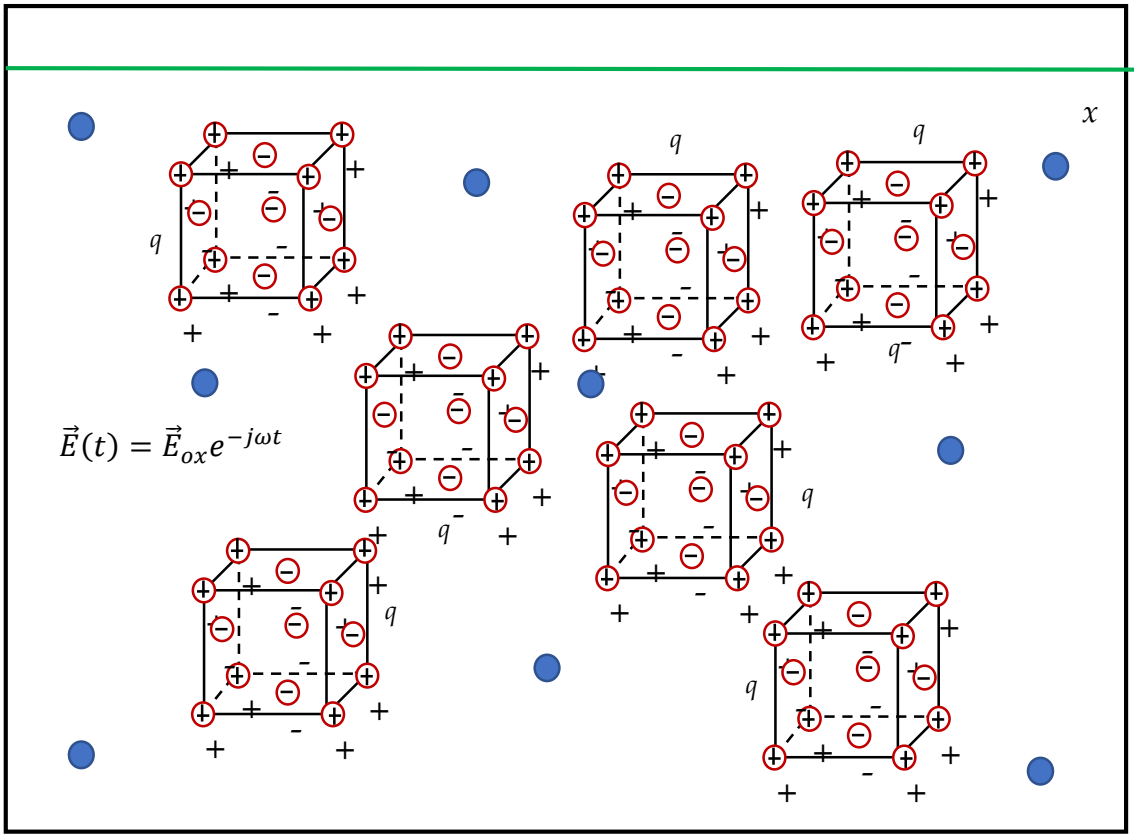

Figure 3. The dilute gas of charged metallic nano-particles (the electrical charge of the single nano-particle is q) immersed into the lattice of the immobile obstacles (depicted with the blue circles) is shown. The entire system is exerted to the external electrical field $\vec{E} = \vec{E}_{ox}e^{-j\omega t}$.

where M and m are the mass of ionic lattice and electron gas of the charged micro-particles respectively, n and τ are respectively the number density of the charged particles

Preprints (www.preprints.org) | NOT PEER-REVIEWED | Posted: 28 March 2022 doi:10.20944/preprints202203.0357.v1

and mean free time between collisions of the charged particles with the immobile "obstacles" respectively. It is seen from Eq. 15 that, when the frequency $\boldsymbol{\omega}$ approaches the plasma frequency $\boldsymbol{\omega_p}$ from above the effective electrical conductivity $\boldsymbol{\sigma}$ will be negative.

Consider the micro-particles in which the charge carriers are electrons. In this case the plasma frequency is given by Eq. 16:

$$\boldsymbol{\omega_p = \sqrt{\frac{\tilde{n}e^2}{\varepsilon_0 m_e}}}, \tag{16}$$

where e, $\boldsymbol{m_e}$ and $\boldsymbol{\tilde{n}}$ are the electrical charge, mass and concentration of electrons respectively [23-25]. Again, we deal with the twin-time scale system, with the characteristic time scales $\boldsymbol{\tau}$ and $\frac{1}{\omega_p}$. The low-frequency, high-frequency limits of electrical conductivity, and the asymptotic value of $\boldsymbol{\sigma}$ in the vicinity of $\boldsymbol{\omega_p = \sqrt{\frac{k}{m}}}$ are given by Eqs. 5-7 in which substitution $\boldsymbol{\omega_0 \to \omega_p}$ is performed. Consequently the refractive index of the model system shown in **Figure 3** us supplied by Eq. 17, which is analogous to Eq. 8.

$$\boldsymbol{n^2(\omega) = 1 + \frac{nq^2\tau}{\varepsilon_0 j\left(M + \frac{m\omega_p^2}{\omega_p^2 - \omega^2}\right)\omega(1 + j\omega\tau)}} \tag{17}$$

The high frequency ($\boldsymbol{\omega\tau \gg 1}$), low frequency $\boldsymbol{\omega\tau \ll 1}$ and asymptotic ($\boldsymbol{\omega \to \omega_p}$) limit expressions for the refractive index are obtained in a complete analogy with Eqs. 9-14 under substitution $\boldsymbol{\omega_0 \to \omega_p}$. For example the low-frequency asymptotic value of the real component of the refractive index, when $\boldsymbol{\omega \to \omega_p}$ is assumed is given by Eq. 18:

$$\boldsymbol{\lim_{\omega\tau \ll 1; \omega \to \omega_p} n_R(\omega) \cong -\sqrt{\frac{nq^2\tau}{2\varepsilon_0 m\omega_p}}\sqrt{\left(\frac{\omega}{\omega_p}\right)^2 - 1}} \tag{18}$$

Eq. 18 is valid when $\boldsymbol{\tau \ll \frac{1}{\omega_p}}$ is adopted. It is recognized from Eq. 18 that $\boldsymbol{n_R(\omega) < 0}$ takes place for the model system presented in Figure 2, when the frequency $\boldsymbol{\omega}$ approaches $\boldsymbol{\omega_p}$ from above; thus, resulting in the negative refraction.

4. Discussion

As it was already mentioned there is no actual negative mass indeed [14]. The effect of the negative effective mass emerges when we substitute the complex mechanical systems comprising a pair of masses (M and m) and ideal spring k by a single effective mass $\boldsymbol{m_{eff}}$, in other words the identity of the internal mass m is ignored and its effect is expressed by the introduction of the mass $\boldsymbol{m_{eff}}$ [11-14]. Introducing of the negative effective mass enables to describe the contra-intuitive situation, when the acceleration of the system is in an opposite direction to the applied force [11-14].At the same time the "imaginary" negative effective mass gives rise to the observable, however, contra-intuitive physical effects, such as negative refraction of acoustic waves and negative bilk modulus [31-32]. We demonstrate that the effect of the negative effective mass also yields the effect of the negative electrical conductivity, when that the electrical current flows against the direction field $\boldsymbol{\vec{E}}$ and correspondingly the electrical force $\boldsymbol{\vec{F} = q\vec{E}}$. The same system built of electrically charges core-spring-shell units, shown in **Figure 1** also gives rise to the negative refraction.

5. Conclusions

Metamaterials are artificial materials, which give rise to the contra-intuitive physical properties, such as negative refraction [1-6, 10]. One of the most unusual effects, which may be involved into the development of the novel metamaterials is the so-called effect of the negative effective mass emerging in the mechanical core-spring-shell systems, in which the core mass m is connected to the shell M with the ideal massless elastic spring k. The effect occurs when the entire system is substituted with the single mass m_{eff}. If the aforementioned core-shell system is exposed to the external harmonic force with a frequency of ω which is close to $\omega_0 = \sqrt{\frac{k}{m}}$ (however, remaining larger than ω_0) the entire system demonstrate the unusual physical behavior, namely the acceleration of the effective mass, representing the entire system, will be in the opposite direction to the applied force [11-14]. We introduced the model ideal gas of the core-shell units which are charged with the excess electrical charge q, embedded into the system of fixed obstacles, resembling the Drude-Lorentz free electron gas [23-25].

When this gas is exposed to the external harmonic electrical field $\vec{E} = \vec{E}_{0x}e^{-j\omega t}$, the core-shell electrically charged units are exerted to the harmonic complex force, given by $\hat{F}(t) = qE_{ox}e^{-j\omega t}$. The entire system (gas of the charged core-shell units) will demonstrate the electrical conductivity $(\omega) = \frac{nq^2\tau}{M+\frac{m\omega_0^2}{\omega_0^2-\omega^2}}$, where n and τ are respectively the number density of core-shell units and mean free time between collisions of the core-shell units with the "obstacles" respectively. The electrical conductivity $\sigma(\omega)$ becomes negative when the exciting frequency ω approaches to $\omega_0 = \sqrt{\frac{k}{m}}$ from above. In principle, the negative conductivity is unrestricted. The suggested model system is characterized by a pair of characteristic time scales, namely τ and $\frac{1}{\omega_0}$. Asymptotic behavior of the electrical conductivity for low and high frequencies is considered. The introduced system demonstrates also the negative refraction in the low-frequency limit; the asymptotic of the refractive index is given in this case by $\lim_{\omega\tau\ll 1;\omega\to\omega_0} n_R(\omega) \cong -\sqrt{\frac{nq^2\tau}{2\varepsilon_0 m\omega_0}}\sqrt{\left(\frac{\omega}{\omega_0}\right)^2 - 1}$. Experimental implementation of the suggested system, exploiting the free plasma oscillations of the electron gas is suggested.

Author Contributions: Conceptualization, E.B.; methodology, E. B.; validation, E. B.; formal analysis, E. B.; investigation, E.B.; writing—original draft preparation, E.B.; writing—review and editing, E.B. All authors have read and agreed to the published version of the manuscript.

Funding: This research received no external funding.

Institutional Review Board Statement: Not applicable.

Informed Consent Statement: Not applicable.
Data Availability Statement: Not applicable.

Acknowledgments:

Conflicts of Interest: The authors declare no conflict of interest.

References

1. Cui, T. J.; Smith, D.; Liu, R. *Metamaterials. Theory, Design, and Applications*, Springer, NY., USA, 2010.
2. Singh, A. K.; Abegaonkar, M. P.; Koul, S. K. *Metamaterials for Antenna Applications*, CRC Press, Boca Raton, Fl. USA, 2022.
3. Felbacq, D.; Bouchitté, G. *Metamaterials Modelling and Design*, Taylor & Francis, Pan Stanford Publishing, Singapore, 2017.
4. Marques, R.; Martin, F.; Sorolla, M. *Metamaterials with Negative Parameters: Theory, Design, and Microwave Applications* (Wiley Series in Microwave and Optical Engineering Book 183), J. Wiley & Sons, Hoboken, USA, 2008.
5. Engheta, N.; Ziolkowski, R. W. *Electromagnetic Metamaterials: Physics and Engineering Explorations*, IEEE Press, Hoes Lane, NJ, USA, 2006.
6. Semouchkina, E. *Dielectric Metamaterials and Metasurfaces in Transformation Optics and Photonics*, Woodhead Publishing, Cambridge, MA, USA, 2021

7. Wu, W.; Hu, W.; Qian, G.; Liao, H.; Xu, H.; Berto, F. *Mechanical design and multifunctional applications of chiral mechanical metamaterials: A review*. *Materials & Design* **2019**, *180*, 107950.
8. Kshetrimayum, R. S. A Brief Intro to Metamaterials. *IEEE Potentials*. **2004**, *23* (5), 44–46.
9. Li, Y., Li, W., Han, T. Fan, S..; Qui S-W. Transforming heat transfer with thermal metamaterials and devices. *Nat. Rev. Mater.* **2021**, *6*, 488–507.
10. Veselago, V. G. The electrodynamics of substances with simultaneously negative values of *e* and *u*. *Sov. Phys. Usp*. **1968**, *10*, 509–514.
11. Milton, G. W.; Willis, J. R. On modifications of Newton's second law and linear continuum elastodynamics. *Proc. R. Soc. A* **2007**, *463*, 855–880.
12. Liu, X.N.; Hu, G. K.; Huang, G. L.; Sun, C. T. An elastic metamaterial with simultaneously negative mass density and bulk modulus. *Appl. Phys. Lett*. **2011**, *98*, 251907.
13. Chan, C. T.; Li, J.; Fung, K. H. On extending the concept of double negativity to acoustic waves. *JZUS A* **2006**, *7*, 24-28.
14. Huang, H. H.; Sun, C. T.; Huang, G. L. On the negative effective mass density in acoustic metamaterials. *Int. J. Eng. Sci*. **2009**, *47*, 610-617.
15. Bormashenko, Ed.; Legchenkova, I. Negative effective mass in plasmonic systems. *Materials* **2020**, *13* (8), 1890.
16. Bormashenko, Ed; Legchenkova, I.; Frenkel, M. Negative Effective Mass in Plasmonic Systems II: Elucidating the Optical and Acoustical Branches of Vibrations and the Possibility of Anti-Resonance Propagation. *Materials* **2020**, *13*(16), 3512.
17. Liu, Z. Y.; Zhang, X. X.; Mao, Y. W.; Zhu, Y.Y.; Yang, Z. Y.; Chan, C. N.; Sheng, P. Locally resonant sonic materials, Science, 2000, 289 (5485), 1734-1736,
18. Valipour, A.; Kargozarfard, M. H.; Rakhshi, M.; Yaghootian, A.; Sedighi, H. M. Metamaterials and their applications: An overview, *Proceedings of the Institution of Mechanical Engineers, Part L* **2021**; *2021*, 1-40.
19. Peralta, I.; Fachinotti, V. D.; Álvarez Hostos, J. C. A Brief Review on Thermal Metamaterials for Cloaking and Heat Flux Manipulation, *Adv. Eng. Mater*. **202**0, *22* (2), 1901034.
20. Liao, G.; Luan, C.; Wang, Z.; Liu, J.; Yao, X.; Fu, J. *Adv. Mater. Techn*. **2021**, *6* (5), 2000787.
21. Lim, C.W. From Photonic Crystals to Seismic Metamaterials: A Review via Phononic Crystals and Acoustic Metamaterials. Arch. Computat. Methods Eng. **2022**, *29*, 1137–1198.
22. Lončar, J.; Igrec, B.; Babić, D. Negative-Inertia Converters: Devices Manifesting Negative Mass and Negative Moment of Inertia, *Symmetry* **2022**, 14(3), 529.
23. Mizutani, U. *Introduction to the Electron Theory of Metals*; Cambridge University Press (CUP): Cambridge, UK, 2001.
24. Kittel, C. *Introduction to Solid State Physics*. Ch. 6., pp. 131-156, 8th Ed. J.Wiley & Sons, Hoboken, NJ, USA, 2005.
25. Feynman, R. *The Feynman Lectures on Physics*, Addison Wesley Publishinng Co. Reading, Massachusetts, Palo Alto, 1964.
26. Shukla, P. K. A survey of dusty plasma physics, *Physics of Plasmas* **2001**, *8*, 1791.
27. Thomas, H.; Morfill, G. E.; Demmel, V.; Goree, J.; Feuerbacher, B.; Möhlmann, D. Plasma Crystal: Coulomb Crystallization in a Dusty Plasma, *Phys. Rev. Lett*. **1994**, *73*, 652.
28. Pustylnik, M. Y.; Pikalev, A. A.; Zobnin, A. V.; Semenov, I. L.; Thomas, H. M.; Petrov, O. F. Physical aspects of dust–plasma interactions, *Contributions to Plasma Physics*, **2021**, *61* (10), e202100126.
29. Jahan, S.; A.; Chowdhury, N. A.; Mannan, A.; Mamun, A. A. Modulated Dust-Acoustic Wave Packets in an Opposite Polarity Dusty Plasma System, *Comm. Theor. Physics*, **2019**, *71* 327.
30. Shapira, Y.; Chaniel, G.; Bormashenko, Ed. Surface charging by the cold plasma discharge of lentil and pepper seeds in comparison with polymers, Colloids & Surfaces B**, 2018**, *172*, 541-544.
31. Sang, S., Mhannawee, A. & Wang, Z. A design of active elastic metamaterials with negative mass density and tunable bulk modulus. *Acta Mech*. **2019**, *230*, 1003–1008.
32. Liu, X. N.; Hu, G. K.; Huang, G. L.; Sun, C. T. An elastic metamaterial with simultaneously negative mass density and bulk modulus. *Appl. Phys. Lett*. **2011**, *98*, 251907.